2015

Hyaluronidase Hyal1 Increases Tumor Cell Proliferation and Motility through Accelerated Vesicle Trafficking

Caitlin O McAtee
University of Nebraska - Lincoln

Abigail R. Berkebile
University of Nebraska-Lincoln

Christian Elowsky
University of Nebraska-Lincoln, celowsky@unl.edu

Teresa Fangman
University of Nebraska-Lincoln

Joseph J. Barycki
University of Nebraska - Lincoln, jbarycki2@unl.edu

See next page for additional authors

THE JOURNAL OF BIOLOGICAL CHEMISTRY VOL. 290, NO. 21, pp. 13144–13156, May 22, 2015

Hyaluronidase Hyal1 Increases Tumor Cell Proliferation and Motility through Accelerated Vesicle Trafficking*

Received for publication, February 22, 2015, and in revised form, April 7, 2015 Published, JBC Papers in Press, April 8, 2015, DOI 10.1074/jbc.M115.647446

Caitlin O. McAtee[‡], Abigail R. Berkebile[‡], Christian G. Elowsky[§], Teresa Fangman[§], Joseph J. Barycki[‡], James K. Wahl III[¶], Oleh Khalimonchuk[‡], Naava Naslavsky[‖], Steve Caplan[‖], and Melanie A. Simpson[‡]**[1]**

*From the [‡]Department of Biochemistry, University of Nebraska, Lincoln, Nebraska 68588, [§]Morrison Microscopy Facility, University of Nebraska, Lincoln, Nebraska 68588, [¶]Department of Oral Biology, University of Nebraska Medical Center College of Dentistry, Lincoln, Nebraska 68503, [‖]Department of Biochemistry and Molecular Biology, University of Nebraska Medical Center, Omaha, Nebraska 68198, and **Fred and Pamela Buffett Cancer Center, Omaha, Nebraska 68198*

Background: Hyal1 is a turnover enzyme for hyaluronan that accelerates metastatic cancer by increasing cell motility.
Results: Hyal1-overexpressing cells have a higher rate of endocytosis that impacts cargo internalization and recycling.
Conclusion: The higher rate of vesicle trafficking increases motility receptor function and nutrient uptake.
Significance: This novel mechanism implicates Hyal1 trafficking in multiple signaling events during tumor progression.

Hyaluronan (HA) turnover accelerates metastatic progression of prostate cancer in part by increasing rates of tumor cell proliferation and motility. To determine the mechanism, we overexpressed hyaluronidase 1 (Hyal1) as a fluorescent fusion protein and examined its impact on endocytosis and vesicular trafficking. Overexpression of Hyal1 led to increased rates of internalization of HA and the endocytic recycling marker transferrin. Live imaging of Hyal1, sucrose gradient centrifugation, and specific colocalization of Rab GTPases defined the subcellular distribution of Hyal1 as early and late endosomes, lysosomes, and recycling vesicles. Manipulation of vesicular trafficking by chemical inhibitors or with constitutively active and dominant negative Rab expression constructs caused atypical localization of Hyal1. Using the catalytically inactive point mutant Hyal1-E131Q, we found that enzymatic activity of Hyal1 was necessary for normal localization within the cell as Hyal1-E131Q was mainly detected within the endoplasmic reticulum. Expression of a HA-binding point mutant, Hyal1-Y202F, revealed that secretion of Hyal1 and concurrent reuptake from the extracellular space are critical for rapid HA internalization and cell proliferation. Overall, excess Hyal1 secretion accelerates endocytic vesicle trafficking in a substrate-dependent manner, promoting aggressive tumor cell behavior.

Prostate cancer is the most frequently diagnosed cancer in men (1). Aggressive and metastatic cancers reorganize and invade local tissue matrix, which contributes to the enhanced potential for survival and proliferation of tumor cells under extreme conditions. Hyaluronan (HA)[2] is an extracellular matrix glycosaminoglycan that consists of repeating disaccharides of glucuronic acid and *N*-acetylglucosamine. Turnover of HA is controlled by activity of its degradation enzymes, the hyaluronidases (Hyals), and its synthesis enzymes, the hyaluronan synthases (HASs). In humans, there are five isoforms of Hyal, Hyal1–4, and PH-20 and three isoforms of HAS, HAS1–3 (for a review, see Ref. 2). Altered expression profiles of the Hyal and HAS proteins have been associated with many types of cancers (3–7). Detection of elevated expression of Hyal1 and concurrent accumulation of HA in biopsies are an indicator of poor prognosis for prostate cancer (8). In a mouse orthotopic model of prostate cancer, the accelerated turnover of HA through overexpression of Hyal1 with or without concurrent expression of HAS isozyme HAS2 or HAS3 increases prostate tumorigenesis and metastatic frequency due in part to enhanced tumor cell motility and cell cycle progression (9).

The mechanisms by which Hyal1 overexpression impacts motility and proliferation of tumor cells are not fully understood. Notably, stable prostate tumor cell lines expressing Hyal1 display altered surface expression of CD44, $\alpha4\beta1$ integrin, and N-cadherin, all of which are critical plasma membrane receptors that transduce signals for adhesion, migration, and proliferation (9–11). HA-overproducing cells with low Hyal1 levels inappropriately sustain activation of ERK and elevation of cyclin-dependent kinase inhibitors, which contribute to a delay in cell cycle progression that is relieved by expression of Hyal1. Moreover, because these cells have less plasma membrane integrin and N-cadherin, restoration of normal receptor function in the presence of Hyal1 potentially contributes to accelerated proliferation and motility.

Interestingly, CD44, $\alpha4\beta1$ integrin, and N-cadherin have all been shown to internalize via the same clathrin-independent route (12) and re-externalize through vesicular sorting processes. It is also known that plasma membrane-associated HA can be internalized from the extracellular matrix into the endocytic pathway (13) in a manner that is dependent on Hyal1 and the cell surface HA receptor CD44 (14). Differential engagement of CD44 by HA polymers *versus* Hyal1-cleaved HA fragments or oligomers, respectively, sustains cellular quiescence

* This work was supported, in whole or in part, by National Institutes of Health Grants R01 CA165574 (to M. A. S.), R01 GM087455 and R01 GM074876 (to S. C.) and by Institutional Development Award 5P30GM106397 from the NIGMS (to M. A. S. and S. C.). This work was also supported by a Nebraska Research Initiative grant (to M. A. S. and S. C.).
[1] To whom correspondence should be addressed: Dept. of Biochemistry, University of Nebraska, N246 Beadle Center, 1901 Vine St., Lincoln, NE 68588-0664. Tel.: 402-472-9309; Fax: 402-472-7842; E-mail: msimpson2@unl.edu.
[2] The abbreviations used are: HA, hyaluronan; HAS, hyaluronan synthase; tdT, tdTomato; fHA, fluorescein-conjugated HA; Hyal, hyaluronidase; ER, endoplasmic reticulum.

or induces internalization of the complex. Treatment of tumor cells with small HA oligomers induces disruption of CD44 complexes and subsequent internalization of CD44 (15). Similarly, treatment of breast cancer cells with HA oligomers causes CD44 internalization and prevents efflux of lactate from the cells (16). Conversely, it was shown that high molecular mass HA (≥1 million Da) inhibited the stimulation of cyclin D1, acting through the CD44 receptor (17).

The mechanism of Hyal1 enzyme secretion was recently examined in murine macrophages, one of the cell types that is most critically dependent on Hyal1 function. In these cells, Hyal1 is secreted via the ER-Golgi pathway where only a small portion of it is mannose 6-phosphorylated for lysosomal targeting (18). Rather, the majority of the protein is released to the extracellular space and is thought to traffic to lysosomes via endocytosis following capture by the cell surface mannose receptor. Enzyme function has been extensively characterized *in vitro* using site-directed mutagenesis and hyaluronidase enzyme kinetics, but the impact of Hyal1 and its functional mutants on vesicle and receptor trafficking in the context of growth and motility has not been examined. Hyal1 is an acid-active endolytic glycosidase that acts on HA or chondroitin sulfate polymers. Glutamate 131 of Hyal1 is a conserved active site residue that serves as a general acid/general base for hydrolytic cleavage of the β-1,4 linkage between *N*-acetylglucosamine and glucuronate. Mutation of this residue to a glutamine (E131Q) results in complete loss of hyaluronidase activity (19). An additional mutant substituting tyrosine 202 with phenylalanine (Y202F) produces a less impaired enzyme with significantly reduced affinity for HA, although it is still catalytically competent if the substrate is saturating. Hyal1E131Q and Hyal1Y202F are thought to be processed and secreted similarly to wild-type Hyal1 based on Western analysis of lysates and conditioned media (19). In this study, we utilized these point mutants to determine whether the phenotypic effects of Hyal1 overexpression in prostate cancer cells are dependent on its catalytic activity and/or ability to bind extracellular substrates.

Because Hyal1 expression is functionally linked to accelerated proliferation and migration, we investigated the molecular mechanisms by which Hyal1 overexpression directly impacts these processes in the tumor cells. In the current study, we hypothesized that elevated Hyal1 could be affecting cell surface receptor function through alterations in endocytic turnover and vesicle sorting in the cell. To test this, we generated cell lines expressing Hyal1 or its point mutants as fluorescent fusion proteins and characterized growth, motility, and the trafficking itinerary of Hyal1 within live cells. In the context of a well established prostate cancer model where HA homeostasis has a profound impact on cancer progression, these studies provide mechanistic insights into Hyal1 function in cancer that are distinct from its function in normal macrophages and other cells.

Experimental Procedures

Reagents and Antibodies—Fluorescein-conjugated HA was purchased from Merck Millipore. Transferrin-Alexa Fluor 633 conjugate, anti-transferrin receptor antibody, LysoTracker Green DND-26, and ER-Tracker Green BODIPY FL glibenclamide were purchased from Life Technologies. Brefeldin A, chloroquine diphosphate salt, and bafilomycin A1 were obtained from Sigma-Aldrich. Anti-Hyal1 rabbit polyclonal was raised against recombinant Hyal1 protein purified from HEK293 conditioned medium and was previously characterized by our laboratory (19). Anti-calnexin and anti-EEA1 were from BD Biosciences, and anti-cathepsin D was from Calbiochem. Secondary antibodies were goat anti-rabbit IRDye800 and donkey anti-mouse IRDye800, both purchased from Rockland Immunochemicals (Limerick, PA). Other reagents were obtained from Fisher Scientific except where indicated.

Cell Culture and Stable Cell Selection—22Rv1 human prostate adenocarcinoma cells were purchased from ATCC (Manassas, VA) and grown in RPMI 1640 medium containing 10% FBS. Culture of 22Rv1 stable transfectants expressing pIRES2-EGFP vector or the constructs encoding unfused Hyal1WT and Hyal1E131Q was as described previously (9, 10). The ptdTomato-N1 vector was purchased from Clontech and was used to create constructs encoding the wild-type Hyal1 and point mutants E131Q and Y202F fused to the N terminus of the tdTomato fluorescent reporter protein (excitation, 554 nm; emission, 581 nm). Following sequence verification, empty vector control (tdTomato (tdT)) and the Hyal1WT-tdT, Hyal1Y202F-tdT, and Hyal1E131Q-tdT constructs were used to transfect 22Rv1 cells via the liposomal reagent FuGENE HD (Promega, Madison, WI). Red fluorescent stable lines were selected from resultant colonies following growth in standard serum-containing medium supplemented with 1.5 mg/ml G418. Expression of tdTomato and Hyal1 fusion proteins was assessed by Western analysis using our rabbit polyclonal anti-Hyal1 antibody and anti-dsRed antibody (Clontech). Three to five lines per construct were selected to express equivalent total Hyal1 fusion protein (data not shown). All stable lines were subsequently maintained in RPMI 1640 medium containing 10% FBS and 1.5 mg/ml G418.

Protein Expression Analysis—An initial comparison of fusion protein expression among stable cell lines was made by Western analysis of crude fractions. Cells were seeded to achieve 70% confluence in 48 h of culture using standard medium with 2% low IgG-containing serum. Conditioned media were removed and concentrated 10-fold for non-reducing Western blotting. Cells were washed with PBS, trypsin-released, pelleted at $1000 \times g$, washed once with PBS, resuspended in PBS containing protease inhibitors, and centrifuged at $15{,}000 \times g$ (15 min at 4 °C). The supernatant was collected as the cytosolic fraction. The pellet was resuspended in PBS with 1% Triton and protease inhibitor mixture, incubated on ice (30 min), and then cleared by centrifugation at $15{,}000 \times g$ (10 min at 4 °C). This supernatant was removed as the membrane- and organelle-enriched fraction.

After gel electrophoresis, proteins were transferred to a PVDF membrane. Membranes were blocked with 5% milk in PBS + 0.1% Tween and probed with anti-Hyal1 rabbit polyclonal (1:1000) or anti-tubulin (1:750,000). After primary incubation, membranes were washed, incubated with IRDye-conjugated secondary antibodies, and then imaged using the LI-COR Odyssey and software.

Proliferation and Motility Assays—To compare rates of proliferation, equal numbers of cells from each of the four stable

tdTomato cell line populations as indicated were seeded in quadruplicate wells of five 96-well plates (3×10^4 cells/ml in 100 μl of serum-containing medium/well). Each day, one set of quadruplicate wells per line was trypsin-released, neutralized, and manually counted in a hemacytometer. Mean cell counts per well were plotted from one representative 5-day assay that was reproduced at least three times. Cells expressing unfused Hyal1WT or Hyal1E131Q in the pIRES2-EGFP vector were assayed similarly but quantified by addition of WST-1 reagent, plotting absorbance at 450 nm. Statistical significance was assessed using Student's two-tailed *t* test.

Motility was measured using a 48-well modified Boyden chemotaxis chamber. Lower wells were loaded with serum-free medium containing 25 μg/ml type IV mouse collagen (BD Biosciences). The upper wells were filled with serum-free medium containing single cell suspensions of each stable line in quadruplicate as indicated (2×10^4 cells) separated from the lower wells by polycarbonate membranes with 8-μm pore size (Neuroprobe Inc., Gaithersburg, MD). After incubating at 37 °C for 21 h, the membrane was removed from the chamber, fixed, stained with the Diff-Quik Stain kit (VWR International, Batavia, IL), and mounted on a glass slide. Unmigrated cells were removed from the top of the membrane with a cotton swab, and the membrane was preserved with Gel Mount and a glass coverslip. Migrated cells were counted in five random fields per well at 20× magnification using a gridded ocular micrometer. Representative data were plotted from an assay reproduced at least three times. Significance was determined by Student's *t* test.

Characterization of Hyal1 Subcellular Localization and Trafficking Itinerary—Cells were seeded in glass bottom culture dishes (MatTek Corp., Ashland, MA) for 24 h prior to imaging or treatment. At 24 h postseeding, live cells were washed with fresh medium and immediately imaged on an Olympus FV500 confocal laser scanning microscope with an Olympus IX81 inverted fluorescence microscope and an Olympus PlanApo 100× oil lens (numerical aperture, 1.45; working distance, 17 mm). To demonstrate subcellular localization of the tdTomato fusion proteins, we incubated cells with live dye tracking agents before washing and imaging. LysoTracker Green DND-26 was used at a concentration of 75 nM for 5 min at 37 °C. ER-Tracker Green BODIPY FL glibenclamide was used at a concentration of 1 μM for 20 min. Imaging of colocalization was performed using a Marianas microscopy system with a Plan-NEOFLUAR 40×, 1.3 numerical aperture objective controlled by SlideBook 5.0 image acquisition software (Intelligent Imaging Innovations Inc., Denver, CO). Colocalization of fluorescent proteins was quantified by importing images ($n = 10–16$) into ImageJ and calculating the Pearson's correlation coefficient for the green channel signal overlaid on the tdTomato signal.

To perturb intracellular trafficking and confirm subcellular localization of Hyal1 fusion proteins, we incubated cells preseeded in glass bottom dishes with specific trafficking inhibitors for the times indicated, washed, and then imaged immediately on the Olympus FV500-IX81 confocal microscope. Brefeldin A was used at a concentration of 10 μg/ml for 1 h at 37 °C. Chloroquine diphosphate salt was used at a concentration of 50 μM for 24 h at 37 °C. Bafilomycin A1 was used at a concentration of 5 nM for 48 h at 37 °C.

Biochemical Fractionation and Western Analysis—Stable transfectants expressing Hyal1WT-tdT, Hyal1Y202F-tdT, or Hyal1E131Q-tdT were incubated in standard medium or treated as above in brefeldin A, chloroquine, or bafilomycin A1. After desired treatments, cells were washed with PBS, scraped off the culture dish, pelleted at 1500 rpm, and resuspended in 0.5 ml of PBS. Cells were lysed by drawing through a 21-gauge needle 20 times. Lysed cells were centrifuged at $800 \times g$ for 10 min at 4 °C to pellet the insoluble fraction. The postnuclear supernatant was then applied to the top of a tube containing a continuous sucrose gradient from 10 to 40% sucrose. The gradient was centrifuged for 6 h at $100{,}000 \times g$ at 4 °C. Fractions of 250 μl each were collected by piercing the bottom of the tube with a needle and allowing the fractions to drip out.

After gel electrophoresis, proteins were transferred to a PVDF membrane. Membranes were blocked with 5% milk in PBS + 0.1% Tween and probed with desired antibodies. Primary antibody dilutions used were as follows: anti-Hyal1 rabbit polyclonal (1:1000), anti-calnexin (1:2000), anti-cathepsin D (2.5 μg/ml), and anti-EEA1 (1:250). After primary incubation, membranes were washed and incubated with IRDye-conjugated secondary antibodies. Membranes were imaged using the LI-COR Odyssey and software.

Rab Colocalization—Stable Hyal1WT-tdT transfectants were transiently transfected with constructs expressing C-terminal GFP fusions with Rab5, Rab7, Rab11, or their constitutively active or dominant negative counterparts. After 48 h, live cells were imaged on the Olympus FV500-IX81 confocal microscope. Colocalization of fluorescent proteins was quantified by importing images into ImageJ and calculating the Pearson's correlation coefficient for the GFP signal overlaid on the tdTomato signal.

Fluorescein-HA Uptake—Stable transfectant lines were seeded in glass bottom dishes overnight, washed in serum-free medium, and incubated for 5 min in 100 nM fluorescein-conjugated HA (fHA) prior to imaging on the Olympus FV500-IX81 confocal microscope. To quantify the impact of HA uptake on Hyal1 distribution, images were imported into ImageJ, and Pearson's correlation coefficient was calculated for HA in green relative to Hyal1 in red. To determine whether secreted Hyal1 was essential for HA uptake, we treated cell lines with brefeldin A for 1 h to suppress ER-Golgi secretion of Hyal1 and repeated the 5-min fHA treatment. Finally, to determine whether Hyal1 HA binding or catalytic activity was essential for HA endosomal internalization, we allowed brefeldin A-treated cells to recover for 30 min and again assayed HA internalization and repeated the image collection and calculation of correlation coefficients.

Transferrin Uptake—Cells were seeded overnight in 10-cm tissue culture dishes, washed in serum-free media, and incubated with transferrin-Alexa Fluor 633 conjugate for the indicated periods of time. Following incubation, cells were washed twice with PBS, released with trypsin, washed twice, and resuspended in PBS for immediate analysis by flow cytometry. Mean fluorescence intensity of the Alexa Fluor 633 signal for the scatter-gated cells was plotted for the uptake time course to illustrate differences among cells.

Results

Hyal1 Increases Proliferation and Motility of Prostate Tumor Cells by a Mechanism That Requires Its Catalytic Competence—We previously reported that 22Rv1 human prostate carcinoma cells selected for stable overexpression of Hyal1 exhibited higher motility and proliferation relative to control lines expressing only the empty vector (9). Of note, cells with high levels of Hyal1 expression also had greater cell surface expression of β1 integrin and N-cadherin and were more adherent to extracellular matrix proteins such as fibronectin and collagen (11). To further examine the mechanism of Hyal1 impact on cellular function, we selected cells that stably expressed wild-type Hyal1, the reduced HA-binding mutant Hyal1-Y202F, or its catalytically inactive point mutant, Hyal1-E131Q (19), as an N-terminal fusion to the tdTomato fluorescent protein encoded with the native N-terminal Hyal1 signal peptide (hereafter referred to as Hyal1WT-tdT, Hyal1Y202F-tdT, and Hyal1E131Q-tdT, respectively). All three fusion proteins were expressed and folded correctly based on the detection of comparable levels in conditioned media and strong expression in lysates (Fig. 1*A*) relative to the distribution profiles of unfused proteins in our previous study (19). Although all three proteins were secreted, subdivision of whole cell lysates into cytosolic and Triton-soluble membrane/organelle-enriched fractions prior to Western analysis revealed all three in the Triton-soluble fractions and minimally cytosolic as previously observed for the unfused proteins. However, similar expression of Hyal1E131Q-tdT in conditioned media relative to the wild-type or Y202F fusions was attained only when lysate levels of the Hyal1E131Q-tdT stable lines were ≈10-fold higher.

As expected, stable Hyal1WT-tdT cells grew and migrated more rapidly than the control vector transfectant (Fig. 1*B*). In contrast, cells overexpressing Hyal1E131Q-tdT did not exhibit accelerated growth or motility (Fig. 1*C*), achieving rates of proliferation and migration that were comparable with those of the empty vector transfectants. These results were consistent with relative proliferation and motility of stable transfectants overexpressing Hyal1WT or Hyal1E131Q native proteins with GFP as a reporter but not as a fusion protein (Fig. 1, *D* and *E*, respectively). Interestingly, the proliferation and migration rates of Hyal1Y202F-tdT cells were enhanced relative to the empty vector controls but not to the extent conferred by overexpression of Hyal1WT-tdT. Thus, the catalytic activity of overexpressed Hyal1 is at least partially responsible for the higher rates of cell growth and migration in 22Rv1 prostate tumor cells, and the effect is potentially dependent on Hyal1 binding efficiency and/or external substrate concentrations.

Vesicular Localization of Hyal1 in Prostate Tumor Cells Is Dependent upon Its Catalytic Activity—We hypothesized that the rate or itinerary of Hyal1 vesicular trafficking may be dictated by its catalytic competence and/or substrate binding potential, which in turn could generally impact cell behavior through the alterations in cell surface integrin and cadherin we showed previously (9–11). Because Hyal1 is important for internalization and lysosomal breakdown of HA, we chose to use the tdTomato fusion as a reporter for studies investigating

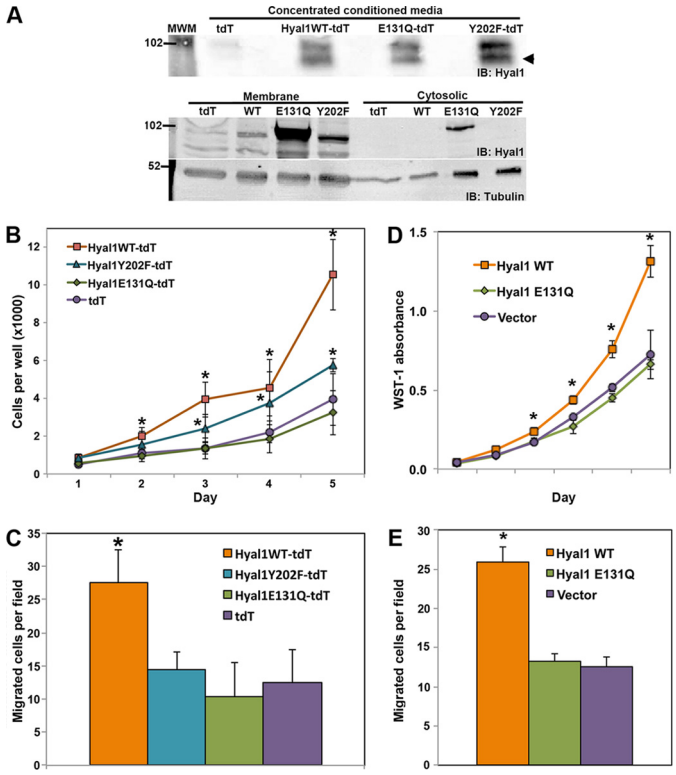

FIGURE 1. **Expression of catalytically active Hyal1 increases proliferation and motility of prostate tumor cells.** 22Rv1 prostate carcinoma cells were selected for stable overexpression of the empty vector encoding the reporter tdT or the wild-type Hyal1 (WT and Hyal1WT-tdT), Hyal1Y202F, or Hyal1E131Q, each as a fusion with tdT. *A*, soluble cell lysates, membrane-enriched fractions, and concentrated conditioned media were analyzed by Western blotting with equal amounts of total protein probed for Hyal1 (fusion protein molecular mass of ≈100 kDa) and normalized to tubulin. The specific band for Hyal1-tdT fusion protein in conditioned media is indicated by an *arrowhead*. *B*, proliferation was assayed by daily manual counts. Equal numbers of cells were seeded in quadruplicate wells of 96-well plates. Cell numbers are plotted as mean ± S.D. (*error bars*). *C*, cell motility was compared using a modified Boyden chamber assay. Lower wells contained type IV collagen as a chemotactic agent. Single cell suspensions were placed in the upper wells separated from the lower wells by a polycarbonate membrane with 8-μm pore size. The mean ± S.D. (*error bars*) is plotted for quadruplicate manual counts per cell line. *D* and *E*, proliferation and motility, respectively, were quantified for 22Rv1 cells stably expressing empty vector (pIRES2-EGFP), Hyal1WT, or Hyal1E131Q unfused proteins as indicated. *, $p <$ 0.01 for Hyal1WT-tdT transfectant values relative to those of the tdT control line. *MWM*, molecular weight markers; *IB*, immunoblot.

the trafficking of Hyal1 within the cell because of the superior pH stability of its fluorescence signal. Examination of the 22Rv1 transfectants by confocal fluorescence microscopy revealed that Hyal1WT-tdT localized within structures resembling endocytic and/or lysosomal vesicles (Fig. 2*A*). Similar results were obtained for the Hyal1Y202F-tdT mutant (Fig. 2*B*), which retains catalytic competence but requires ≈5-fold higher HA concentrations for maximal activity. In contrast, the Hyal1E131Q-tdTomato protein appeared diffusely in the cytoplasm in a networked structure suggestive of ER localization (Fig. 2*C*). The control tdTomato was distributed throughout the cytoplasm and nucleus (Fig. 2*D*). In some cases, Hyal1WT-tdT could be seen associated with focal contacts at the cell surface, a phenomenon that was not seen in the tdTomato or Hyal1E131Q-tdT transfectants. These results indicate that the catalytic activity of Hyal1 affects its localization within the cell. Specifically, the distribution of Hyal1 coincided more promi-

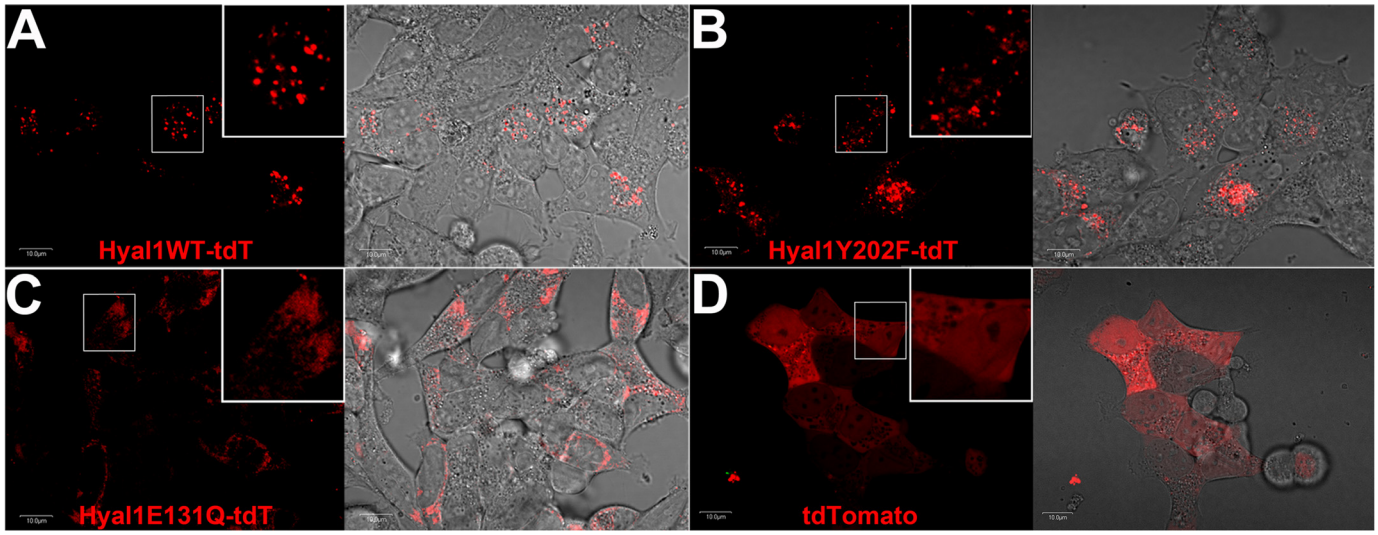

FIGURE 2. **Subcellular distribution of Hyal1 is affected by its catalytic competence.** Stable 22Rv1 cell lines expressing an empty vector encoding the tdTomato fluorescent reporter or C-terminal fusion constructs of tdTomato with wild-type or mutant Hyal1 were imaged by live cell confocal fluorescence microscopy. Red fluorescence (*left panel* of each set) indicates localization of Hyal1WT-tdT fusion protein (*A*), Hyal1Y202F-tdT (*B*), Hyal1E131Q-tdT (*C*), or tdTomato protein (empty vector; *D*). *Inset panels* are zoomed images of the individual cells designated by a corresponding *white square*. In the *right panels* of each set, red channel fluorescence is superimposed on the corresponding transmitted light image. *Scale bars*, 10 μm.

nently with the ER and minimally in endocytic vesicles when the catalytic activity was abolished with no evidence of cell surface or internal punctate structures. These observations support a specific requirement for Hyal1 catalytic activity both in normal secretion of Hyal1 protein by the cell and in the intracellular compartmentalization of the Hyal1 enzyme.

Catalytically Active Hyal1 Is Found in Vesicular Compartments That Localize with Lysosomal and Endosomal Markers—We further examined Hyal1 fusion proteins in combination with live cell organelle tracking dyes. Imaging of cells stained with LysoTracker Green revealed partial overlap of Hyal1WT-tdT fluorescence with the green lysosomal signal represented in *yellow* (Fig. 3*A*; Pearson's correlation coefficients are shown in Fig. 3*F*). There was no detectable merge of Hyal1WT-tdT signal with fluorescent green ER-Tracker (Fig. 3*B*). Similar results were obtained with the Hyal1Y202F-tdT-transfected cells (Fig. 3, *C*, *D*, and *F*). In contrast, red staining of the Hyal1E131Q-tdT fusion protein partially colocalized with green ER-Tracker (*yellow* areas) but not significantly with LysoTracker (Fig. 3*E* and not shown). Strong overlap of signals is shown quantitatively by calculation of Pearson's coefficients for Hyal1WT-tdT (r = 0.68 ± 0.05) and Hyal1Y202F-tdT (r = 0.67 ± 0.07) with LysoTracker and Hyal1E131Q-tdT (r = 0.75 ± 0.04) with ER-Tracker (Fig. 3*F*). To confirm the subcellular compartmentalization of Hyal1WT and mutant enzymes, we performed sucrose density gradient centrifugation of the three cell lines and analyzed the resultant fractions by Western blotting (Fig. 3*G*). Hyal1 has been shown previously to be expressed as a single polypeptide of ~52 kDa in its constitutively secreted form that is endosomally reinternalized in a clathrin-dependent manner and subsequently becomes proteolyzed into two bands of 52 and 48 kDa as vesicles mature to acidified lysosomes. Consistent with this observation, we find that polyclonal Hyal1 antibodies detect two bands for the Hyal1 fusion protein that are separated by an ≈4-kDa molecular mass difference (observed in Hyal1WT and both mutant Western fractions; Figs. 3*G* and 4, *G* and *H*). The Hyal1 band consistent with the intact secreted mass of Hyal1-tdT is ~100 kDa and can be observed to co-fractionate in all three cell lines with EEA1 (fractions 4–6), cathepsin D (two bands; fractions 13–17), and calnexin (fractions 13–19), which correspond to fractions of early endosomes, lysosomes, and microsomes (ER), respectively. However, close comparison of the fractions reveals a greater portion of uncleaved enzyme species in the Hyal1E131Q-tdT cell line that specifically extends throughout the denser fractions (fractions 14–19) of the sucrose gradient in contrast to the wild-type and Y202F mutant, which are more similar to the profile of cathepsin D fractions (fractions 13–17). These results support an active role in vesicular trafficking by catalytically active Hyal1 cargo. The partial unique localization of Hyal1 to non-lysosomal vesicles is consistent with its presence in early or late endosomes in transit from the plasma membrane.

Active Hyal1 Protein Is Secreted via the ER-Golgi Pathway and Endosomally Reinternalized—To elucidate the trafficking itinerary of Hyal1 within the cell, we chemically manipulated commonly used trafficking pathways. First, brefeldin A was used to inhibit protein movement from the ER to the Golgi (20). As a positive control, 22Rv1 cells treated with and without brefeldin A were fixed, permeabilized, and stained with anti-transferrin receptor. Treatment with brefeldin A caused a dramatic visual shift in transferrin receptor localization from primarily punctate structures to a more dense and centralized staining pattern consistent with perinuclear ER networks, suggesting that the trafficking to the Golgi has been inhibited (not shown). When the same treatment was used on 22Rv1 stable lines expressing Hyal1WT-tdT, no difference was seen with or without brefeldin A (Fig. 4, *A*, *B*, and *E*). Similarly, sucrose gradient fractionation of Hyal1WT-tdT cells after brefeldin A treatment showed no shift in localization compared with untreated cells (Fig. 4*G*). Cells expressing Hyal1Y202F-tdT bore a similar punctate intracellular appearance to the Hyal1WT-tdT cells with an overall greater indication of diffuse

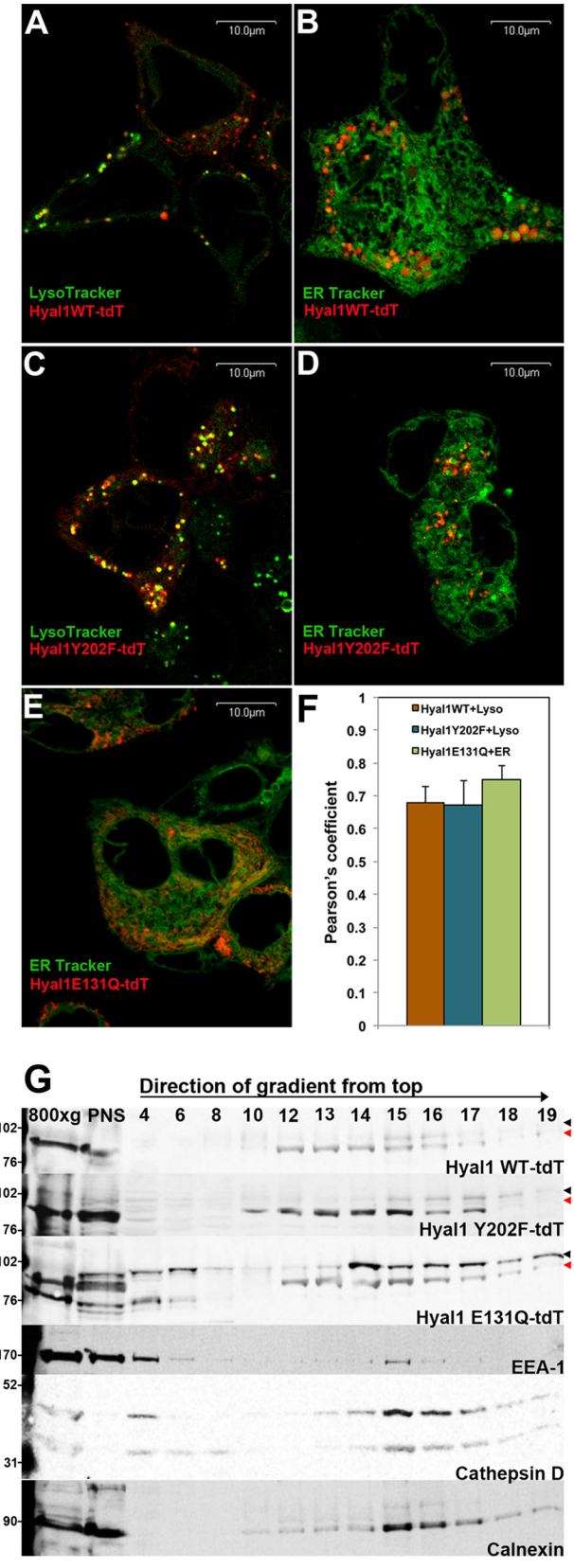

FIGURE 3. **Characterization of intracellular Hyal1 distribution by confocal microscopy and biochemical fractionation.** *A–F*, still images of live 22Rv1 cells expressing Hyal1WT-tdT (*A* and *B*), Hyal1Y202F-tdT (*C* and *D*), or Hyal1E131Q-tdT (*E*) were captured by confocal microscopy following treatment with either LysoTracker Green DND-26 (*A* and *C*) or ER-Tracker Green BODIPY FL glibenclamide (*B*, *D*, and *E*). *Yellow* color represents colocalization of signals. Strong colocalization of Hyal1WT-tdT and Hyal1Y202F-tdT was observed with LysoTracker Green (*Lyso*), whereas the Hyal1-E131Q-tdT merged with ER-Tracker Green (*ER*) as indicated by Pearson's correlation coefficient (*F*). *Error bars* indicate S.E. *G*, stable 22Rv1 transfectants expressing Hyal1WT-tdT or Hyal1E131Q-tdT were lysed and fractionated on a continuous sucrose gradient. Fractions were collected and analyzed by Western blotting with anti-Hyal1 polyclonal antibody. Blots were stripped and reprobed with antibodies to cathepsin D (lysosomes), calnexin (ER), and EEA1 (early endosomes). In each panel, *MWM* is the molecular weight marker, *800×g* is the insoluble fraction of the cell lysate, and *PNS* indicates a sample of the post-nuclear supernatant (soluble lysate) that was loaded on the gradient. *Numbers* correspond to the density fraction following centrifugation. *Increasing numbers* indicate increasing density. *Scale bars*, 10 μm.

fluorescence upon brefeldin A treatment suggestive of some ER accumulation of the fusion protein, whereas Hyal1E131Q-tdT did not show a significant change in localization because this protein was already primarily localized to the ER (Fig. 4, *A*, *B*, and *F*). However, the ER-localized signal was slightly more intense in the presence of brefeldin A treatment. Although there was no obvious shift of the Hyal1E131Q-tdT protein into the denser fractions of the sucrose gradients after brefeldin A treatment (Fig. 4*H*), there was increased intensity of the higher molecular mass band in all fractions, consistent with accumulation of the canonical secretion product. Thus, the inactive mutant fusion protein is likely secreted by this pathway but at a slower rate than the wild type. These results indicate that the normal trafficking mechanism for internalized Hyal1 protein includes trafficking from the ER to the Golgi that is dependent upon the catalytic activity and/or substrate affinity of Hyal1.

Inhibition of Lysosomal Acidification Causes Buildup of Hyal1 Wild-type Protein—To further assess a lysosomal destination for Hyal1, we treated the 22Rv1 stable lines with chloroquine, which inhibits maturation of lysosomes by preventing acidification (21). Chloroquine treatment of either Hyal1WT-tdT or Hyal1Y202F-tdT transfectants resulted in accumulation of larger sized red channel vesicles (Fig. 4, *C*, *E*, and *F*). Sucrose gradient fractionation confirmed that chloroquine treatment induced a shift in the content of Hyal1WT-tdT (fractions 12–17 in Fig. 4*G*) to higher density fractions (fractions 13–19) as well as a small portion localized to the least dense fractions 4 and 6. Moreover, the lower molecular mass band decreased in intensity, consistent with reduced cleavage of Hyal1 as occurs in acidified vesicles. These results suggest that Hyal1 was prevented from following its normal trafficking itinerary to lysosomes where it would function to degrade HA and other glycosaminoglycans and is itself subject to proteolysis. Chloroquine treatment of the 22Rv1 Hyal1E131Q-tdT cells did not alter the fluorescence distribution because significantly lower amounts of the inactive mutant are in vesicles (Fig. 4*C*). However, there was reduced Hyal1 fusion protein in all fractions, and in particular, the lower molecular mass band associated with lysosomal activation was absent (Fig. 4*H*).

Hyal1 Intracellular Trafficking Overlaps with Autophagic Vesicle Formation—To determine whether vesicles containing Hyal1 were involved in autophagy, we treated 22Rv1 stable lines with bafilomycin A1, which prevents the fusion of autophagosomes with lysosomes by inhibiting the vacuolar ATPase that acidifies these vesicles during their maturation (22, 23). When 22Rv1 Hyal1WT-tdT or Hyal1Y202F-tdT cells were treated

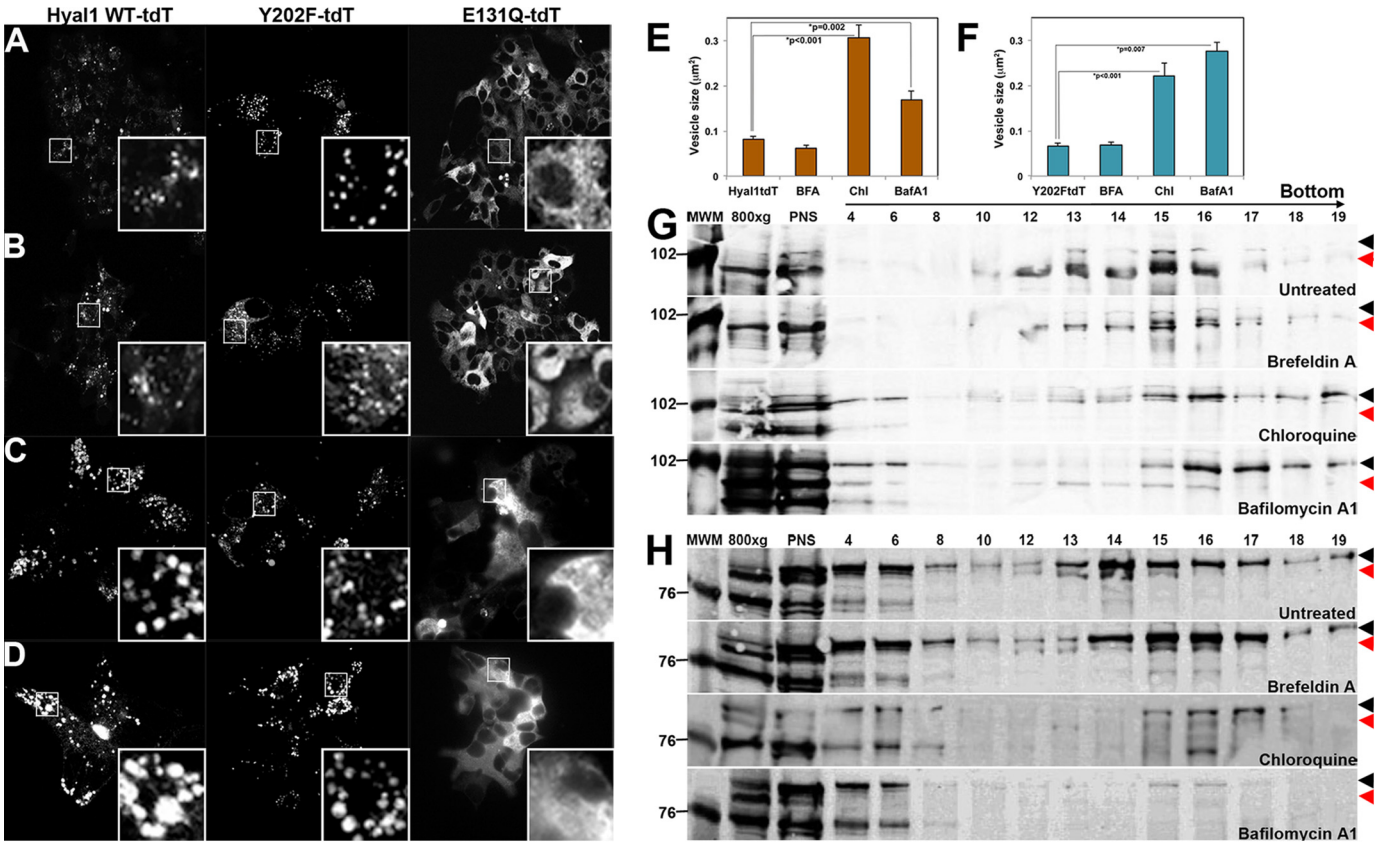

FIGURE 4. **Examination of Hyal1 trafficking itineraries by chemical inhibition of vesicular transport or vesicle acidification.** *A–D*, stable 22Rv1 cell lines expressing Hyal1-tdTomato fusions were incubated in the absence (*row A*) or presence of brefeldin A (*BFA*) (*row B*), chloroquine (*Chl*) (*row C*), or bafilomycin A1 (*BafA1*) (*row D*). Representative images of cells are shown from cultures of Hyal1WT-tdT (*left column*), Hyal1Y202F-tdT (*center column*), and Hyal1E131Q-tdT (*right column*). *Inset panels* show magnified images of individual cells designated in *white squares*. Images are presented with red channel fluorescence isolated in black and white to increase sensitivity of visualization and facilitate analysis. Average vesicle sizes for Hyal1WT-tdT (*E*) and Hyal1Y202F-tdT (*F*) were quantified and compared in each condition. *Error bars* indicate S.E. Statistical significance is indicated on the graphs. Hyal1WT-tdT (*G*) and Hyal1E131Q-tdT (*H*) cells were cultured in standard media or the indicated inhibitor, then lysed, and fractionated by centrifugation on a continuous sucrose gradient. In each panel, *MWM* is the molecular weight marker, *800×g* is the insoluble fraction of the cell lysate, and *PNS* indicates a sample of the postnuclear supernatant (soluble lysate) that was loaded on the gradient. *Numbers* correspond to fractions of increasing density following centrifugation. Fractions were analyzed by Western blotting with the polyclonal anti-Hyal1 antibody. *Arrows* indicate bands corresponding to the full-length (*black*) and processed (*red*) forms of Hyal1.

with bafilomycin A1, there was a significant increase in the size of Hyal1-positive vesicles within the cell (Fig. 4*D*). In the case of Hyal1Y202F-tdT, the substrate-binding mutant, there was a large decrease (54 ± 5%, $p < 0.001$; data not shown) in the number of vesicles per cell. Bafilomycin A1 treatment also caused an accumulation of the unprocessed higher molecular mass Hyal1WT-tdT protein in more dense sucrose gradient fractions 16–19 and in the least dense fractions 4 and 6 (Fig. 4*G*). This suggests that the autophagosomes and lysosomes containing Hyal1 no longer fuse. As expected, bafilomycin A1 treatment had no effect on the fluorescence pattern of Hyal1E131Q-tdT (Fig. 4*D*). However, the fusion protein is significantly reduced in all fractions of the gradient, and only the uncleaved higher molecular mass species is present, primarily in endosomal fractions 4 and 6. Collectively, results are consistent with internalized Hyal1 being directed partially to lysosomes, a portion of which subsequently contribute to autophagic turnover and autophagosome maturation.

Colocalization of Hyal1 with Rab GTPases Demonstrates Its Presence during Endocytosis and Slow Recycling as Well as Late Endosome to Lysosome Maturation—To further characterize the trafficking itinerary of Hyal1, we transiently transfected stable Hyal1WT-tdT cells with constructs encoding GFP fusions to specific Rab GTPases that regulate the sorting of intracellular vesicles. Based on the results of sucrose fractionation, we chose to test Rab5 to identify early endosomes, Rab7 to mark late endosomes and lysosomes, and Rab11 to visualize recycling vesicles. Hyal1WT-tdT red fluorescence overlapped strongly with signals from Rab5-GFP (Fig. 5, *A* and *D*; Pearson's coefficient $r = 0.51 \pm 0.14$) and Rab7-GFP (Fig. 5, *B* and *D*; $r = 0.68 \pm 0.08$), indicating a significant presence of Hyal1 in early endosomes, late endosomes, and lysosomes. Some signal overlap was also observed with Rab11-GFP (Fig. 5, *C* and *D*; $r = 0.31 \pm 0.11$), which suggests that a portion of Hyal1 is sorted to recycling vesicles that return cargo to the cell surface and/or release it to the extracellular space. We next sought to test the effects of perturbing vesicle sorting on Hyal1 localization using previously characterized constitutively active or dominant negative point mutants of each Rab-GFP fusion. Both constitutive activation of Rab5 and dominant negative Rab7 prevent conversion of late endosomes to lysosomes. In each of these images, there is an increased presence of colocalized signal in punctate structures, including several instances in which there appears to be luminal red Hyal1 fluorescence encircled by green Rab5 or

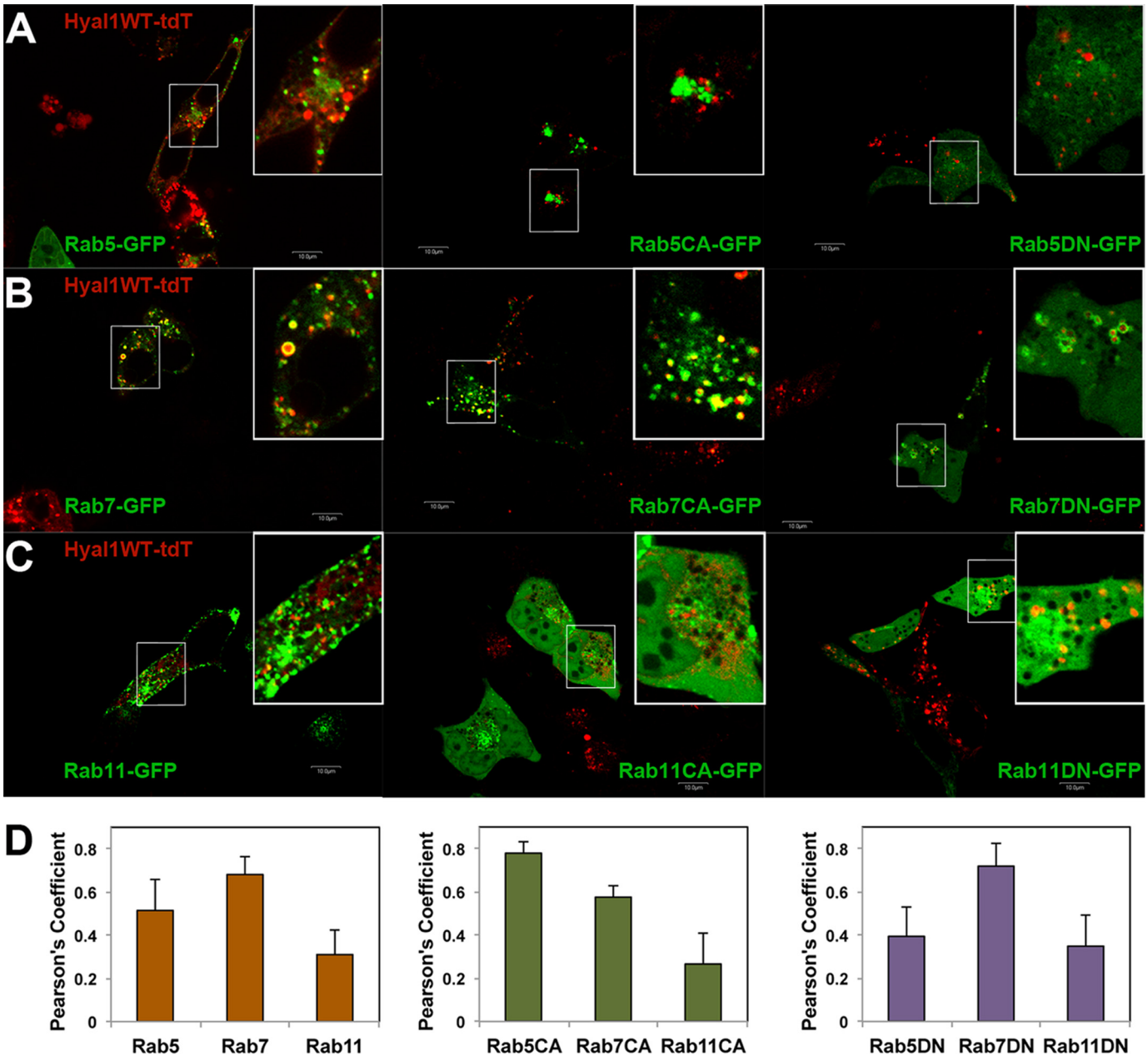

FIGURE 5. **Colocalization of wild-type Hyal1 with Rab GTPases demonstrates its presence in endocytic and slow recycling vesicles as well as late endosomes and lysosomes.** Stable Hyal1WT-tdT cells were transfected with constructs encoding GFP fusions to Rab5, Rab7, or Rab11. Colocalization of each Rab protein is shown by confocal imaging of Rab-GFP fusions (*green*) and Hyal1-tdT fusions (*red*) for Rab5 (*A*), Rab7 (*B*), and Rab11 (*C*). *Yellow* color indicates colocalization. Each set of images shows colocalization of wild-type Rab (*left column*), constitutively active (*CA*) Rab (*center column*), or dominant negative (*DN*) Rab (*right column*). *Inset panels* are magnified images of individual cells indicated by *white squares*. *D*, colocalization of Hyal1WT-tdT with each Rab-GFP construct was quantified by Pearson's coefficient and plotted as mean ± S.E. (*error bars*). *Scale bars*, 10 μm.

Rab7 fluorescence. This is further evidence of endosomally internalized Hyal1 being trafficked from early to late endosomes, ultimately maturing to lysosomes. Dominant negative Rab11, which contributes to the arrest and accumulation of recycling vesicles, showed increased colocalization with Hyal1WT-tdT relative to wild-type Rab11, which supports the slow recycling of a portion of Hyal1 back to the cell surface for re-externalization.

Hyaluronan Uptake Requires Catalytically Active Hyal1, and Internalized HA Vesicles Colocalize with Hyal1—We next wanted to examine the effect of exogenous substrate presence on intracellular Hyal1-tdT distribution because extracellular HA has been shown to internalize via endocytosis in a manner dependent upon Hyal1 (14). Addition of fHA to the culture media of Hyal1WT-tdT and Hyal1Y202F-tdT for 5 min followed by fluorescence confocal microscopy imaging produced significant green fluorescent puncta indicative of endosomal HA uptake (Fig. 6, *A* and *B*). This signal merged with red fluorescent tdT puncta as quantified by Pearson's correlation coefficient, indicating colocalization of HA and Hyal1. In contrast, no evidence of fHA uptake was detected in any images of Hyal1E131Q-tdT or empty vector tdT transfectants (Fig. 6, *C* and *D*). Thus, not only is expression of Hyal1 necessary for HA internalization as shown previously, but these data show that

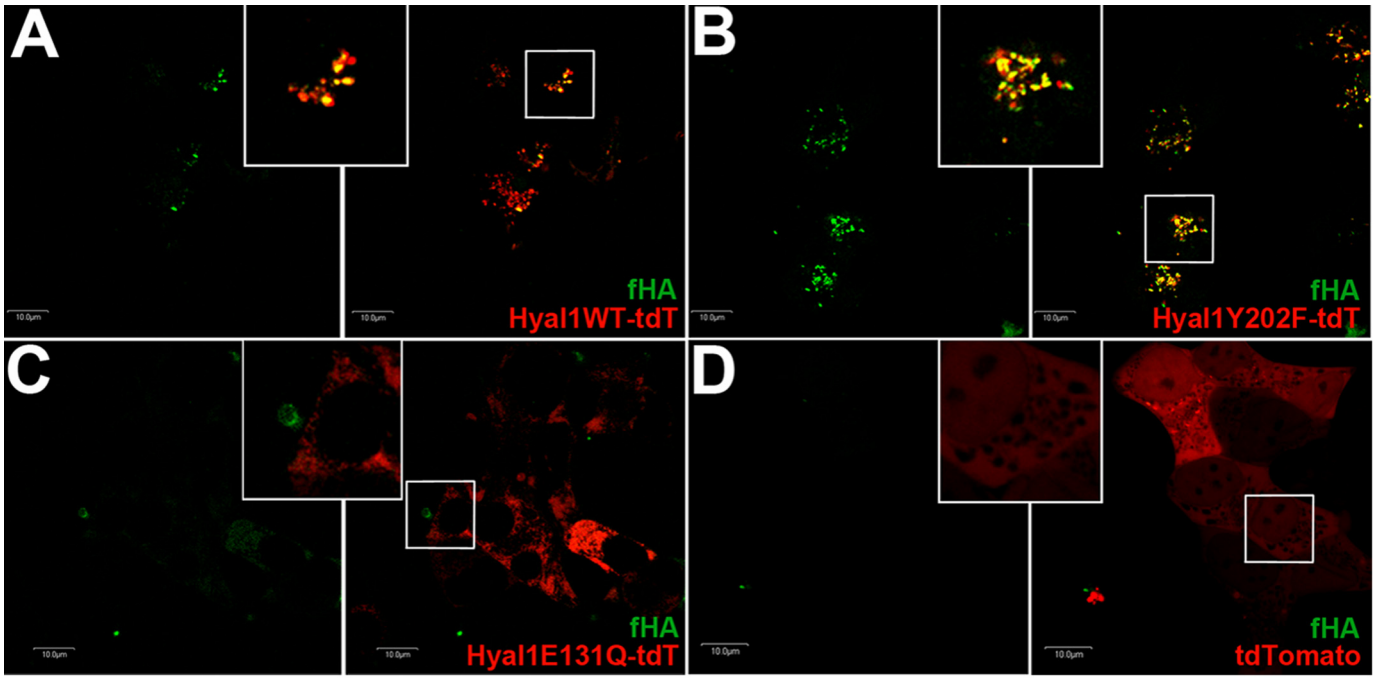

FIGURE 6. **Hyaluronan internalization requires catalytically active Hyal1, and internalized HA vesicles colocalize with Hyal1.** Confocal images are shown for uptake of fHA (*green*) by prostate tumor cells stably expressing Hyal1WT-tdT (*A*), Hyal1Y202F-tdT (*B*), Hyal1E131Q-tdT (*C*), or empty vector (*D*; tdTomato). *Left panels* show fHA uptake alone in *green*, and *right panels* are the corresponding merge. *Inset panels* are magnified images of individual cells designated by *white squares* in the merged panels. *Scale bars*, 10 μm.

the internalized vesicular HA is coincident with Hyal1-positive vesicles.

Extracellular Hyal1 Secretion Is Required for HA Internalization—Hyal1 enzymatic activity appeared to be required for HA uptake (Fig. 6), but the altered secretion profile of the Hyal1E131Q-tdT mutant relative to the wild-type enzyme could also be a factor in the failure of the mutant Hyal1-expressing cells to internalize HA. To distinguish between these possibilities, we re-examined HA uptake following a 1-h treatment of cells with brefeldin A to block secretion of Hyal1 protein from the cell. The treatment was either immediately followed by addition of fHA to the culture media and subsequent image collection or by a 30-min recovery period prior to addition of fHA and image capture. Comparison of fHA (*left inset panels*) and Hyal1-tdT (*right inset panels*) signal patterns in brefeldin A-treated cells relative to untreated cells (Fig. 7, *A* and *B*) reveals significantly reduced uptake of HA in both Hyal1WT-tdT and Hyal1Y202F-tdt transfectants, although tdT signal intensity and distribution do not appear to change, consistent with distribution patterns in Figs. 4 and 6. Also as expected, HA was not internalized in any condition by Hyal1E131Q-tdT transfectants, nor was distribution of the tdT fluorescence altered from its networked appearance. However, after a short recovery period following brefeldin A treatment, significantly increased numbers of small internal puncta in which fHA and tdT fluorescence are merged could be seen in Hyal1WT-tdT transfectants relative to the Hyal1Y202F-tdT HA-binding mutants (Fig. 7*C*). These results (quantified in Fig. 7*D*) confirm that the concurrent uptake of HA and Hyal1 from the extracellular space is required for Hyal1 internalization and provide the novel indication that ligand binding to Hyal1 is a critical prerequisite for uptake.

Stable Hyal1 Expression Increases Rates of Endocytic HA Uptake and Transferrin Internalization by Prostate Tumor Cells—Finally, we evaluated whether the rate of HA uptake and the overall rate of endocytosis differed in the 22Rv1 stable lines. To do this, we incubated single cell suspensions with subsaturating fHA concentrations and monitored the time-dependent fluorescence increase in the cell population by flow cytometry. Consistent with the confocal microscopy data, Hyal1E131Q-tdT and tdTomato control transfectants did not appreciably internalize fHA at any time point. However, cells expressing Hyal1WT-tdT or Hyal1Y202F-tdT internalized HA to an equal extent with similar rates of uptake. Loss of the fluorescein signal occurred rapidly (within 15 min) in the Hyal1WT-tdT uptake assays, consistent with active degradation of fHA by Hyal1 upon internalization and delivery to acidified vesicles. We then measured the overall endocytic rate by incubating cells with fluorescently labeled transferrin, which is a frequently used reporter of clathrin-dependent internalization rates. Initial uptake of labeled transferrin occurred in all stable lines after only 5 min of incubation (Fig. 8*B*) and increased up to 30 min. However, the magnitude of signal increase was significantly higher in cells expressing Hyal1WT-tdT or Hyal1Y202F-tdT than with either of the lines that lack Hyal1 activity. Thus, HA homeostasis directly influences the rate of transferrin uptake in prostate tumor cells, suggesting an overall effect on endocytic uptake and trafficking in these cells. Moreover, the increased uptake of HA and transferrin is likely a mechanism by which the tumor cell could acquire and sequester resources such as carbohydrate and iron that promote the increased proliferation and motility observed in the Hyal1-overexpressing cells.

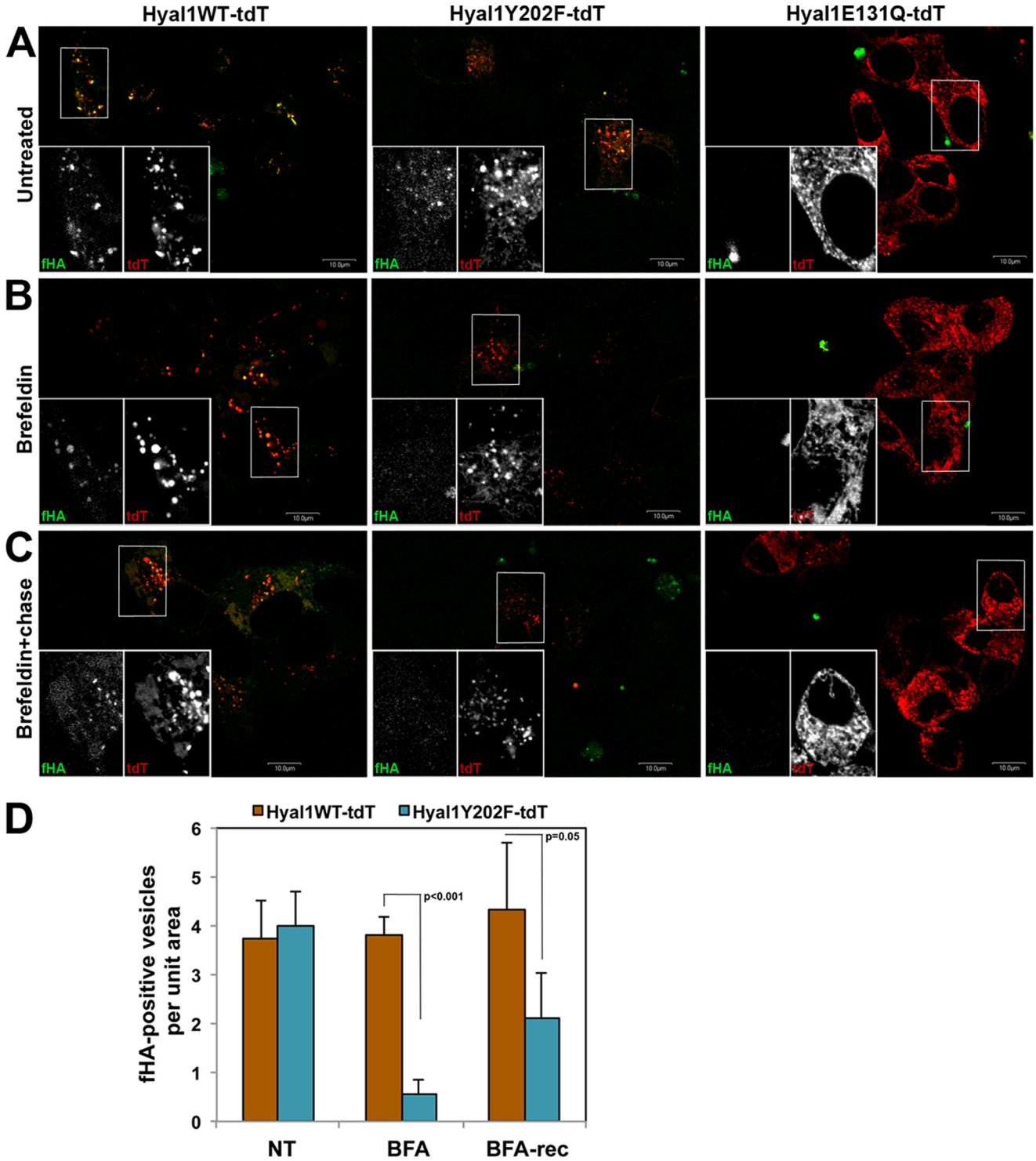

FIGURE 7. **Secreted Hyal1 is essential for efficient HA internalization.** Stable 22Rv1 lines were incubated with fHA without prior treatment (*A*), immediately following treatment with brefeldin A (*B*), or after treatment with brefeldin A followed by a 30-min chase with media to allow recovery (*C*). In each *row*, representative Hyal1WT-tdT cell images are in the *left column*, Hyal1Y202F-tdT images are in the *center column*, and Hyal1E131Q-tdT images are on the *right*. *Inset panels* are magnified images of individual cells designated by *white squares* in the merged panels. The *left inset* shows the isolated green channel fluorescence in black and white indicating fHA uptake, and the *right inset* is the corresponding red channel signal indicating tdT localization. *D*, number of green vesicles per cell was determined using ImageJ for at least 10 cells per condition, each repeated three times and compared for statistical significance by one-way analysis of variance. *Error bars* indicate S.E. *Scale bars*, 10 μm. *NT*, no treatment; *BFA*, brefeldin A; *rec*, recovery.

Discussion

Invasive prostate cancer is clinically associated with elevation of Hyal1 expression, which predicts biochemical recurrence after resection, and Hyal1 overexpression functionally accelerates metastatic progression of orthotopic prostate tumors in mice by increasing rates of proliferation and migration. Based on our previous findings that the distribution and signaling of multiple cell surface receptors were altered signif-

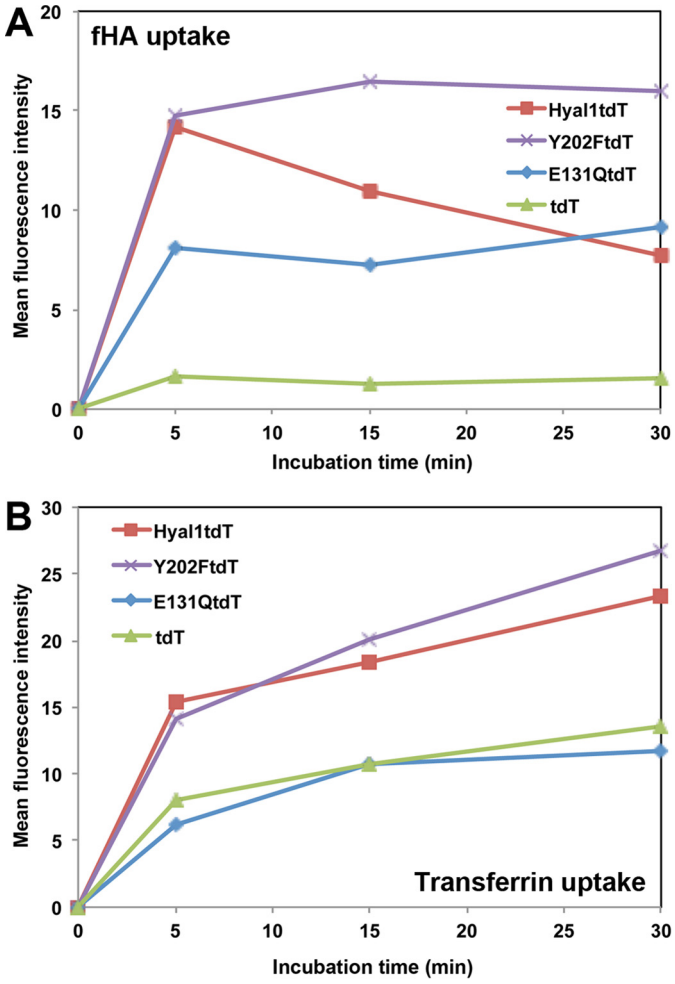

FIGURE 8. **Stable Hyal1 expression increases rates of HA uptake and transferrin internalization by prostate tumor cells.** *A*, single cell suspensions of 22Rv1 prostate tumor cells stably expressing empty vector (tdT), Hyal1WT-tdT, Hyal1Y202F-tdT, or Hyal1E131Q-tdT were incubated in serum-free media (negative) or with media containing 100 nM fHA for the indicated times. HA uptake was monitored via internalized fluorescence intensity using flow cytometry. *B*, prostate tumor cells in *A* were incubated in serum-free media (negative) or with media containing 2.5 μg/ml transferrin-Alexa Fluor 633 for the incubation times indicated, and transferrin uptake was monitored via internalized fluorescence intensity using flow cytometry. In both panels, mean fluorescence intensity as plotted is 1000× higher than the value on the *axis* for presentation. Data are representative of experiments repeated at least four times each.

icantly in Hyal1-overexpressing prostate tumor cells, we tested the hypothesis that intracellular vesicular trafficking was perturbed by excessive catalytic activity of Hyal1. Here, we have shown that rates of endocytosis for both substrates (*e.g.* HA) and non-substrates (*e.g.* transferrin) are increased by Hyal1 expression and that this effect specifically requires Hyal1 catalytic competence. Moreover, we found that the correct trafficking itinerary of Hyal1 involves its secretion through the canonical ER-Golgi pathway to the extracellular space followed by endocytosis-mediated reuptake, vesicular sorting within the cell, and re-externalization of a portion through Rab11-mediated slow recycling with the majority present in Rab5-positive early endosomes or Rab7-positive late endosomes/lysosomes. Interestingly, although the catalytic activity of Hyal1 is not absolutely required for a portion of the Hyal1 to reach the extracellular space, it is required for its efficient reuptake in vesicles and for the appreciable uptake of its substrate, HA.

HA homeostasis could be affecting multiple pathways within the cell directly by influencing the endocytic rate and thereby affecting the cell's access to resources internalized in this manner. Elevated internalization of HA has been shown to provide greater access to sugars that can be shunted through altered metabolic pathways to produce energy through aerobic glycolysis (24), also accelerating growth of tumor cells by allowing the partially oxidized carbohydrate skeletons into biosynthetic pathways. Increased access to amino sugars through this degradation pathway additionally fuels reversible epigenetic modifications such as *N*-acetylglucosaminylation of histones, which has broad ranging effects on gene expression and metabolic repatterning (25, 26).

Transferrin trafficking has similarly been shown to contribute to cell survival and growth promotion in cancer through elevated provision of iron to iron-dependent protein biosynthesis and redox-regulated antioxidant pathways (27). In fact, transferrin may have clinical utility in targeting tumor cells with antiapoptotic agents (28), which our study suggests would be enhanced in tumors that overexpress Hyal1 and/or by concurrent delivery of Hyal1 through accelerated endocytosis.

In addition to cellular resource-promoted effects, there could also be specific impacts on cell signaling downstream of receptor endocytosis. Cell surface receptors that toggle between the plasma membrane and intracellular vesicles to preserve signaling sensitivity in the presence of continuous ligand (*e.g.* EGF receptor; for a review, see Ref. 29) can sustain signaling even while being a component of the endocytic vesicle. Recycling of integrins via endosomal internalization at the trailing edge, trafficking through the cell, and re-externalization at the leading edge is critical for directional cell motility (30–32). It was shown that β1 integrin recycling during cell migration occurs in vesicular compartments and is regulated by specific Rab GTPases (33, 34) that are distinct from the endosome-to-lysosome route followed by internalized material being degraded. Recycling of receptors is determined in part by endosomal pH drop, which differentially dissociates alternate ligands (33, 35). Differences in signaling activation and/or intensity may accompany the internalization of receptors, and this could also influence the proliferation, motility, and other aggressive properties of the cells. These receptors could be eventually degraded in lysosomes or recycled back to the cell surface and available for ligand binding again. The specific fate of unique cell surface receptors in the context of HA turnover remains to be elucidated.

An intriguing implication of our study is that internalized HA appears to have two fates by virtue of its requisite association with Hyal1. A portion of it is clearly directed to complete lysosomal degradation through a combination of Hyal1 activity, which yields a tetrasaccharide as its terminal product that is acted on in lysosomes by exoglycosidases. However, an additional portion has the potential to remain associated with Hyal1 during the sorting to slow recycling vesicles and secreted back to the extracellular space as Hyal1 is re-externalized (Fig. 9). This partially processed material could then have increased affinity for cell surface HA receptors on neighboring cells. Small

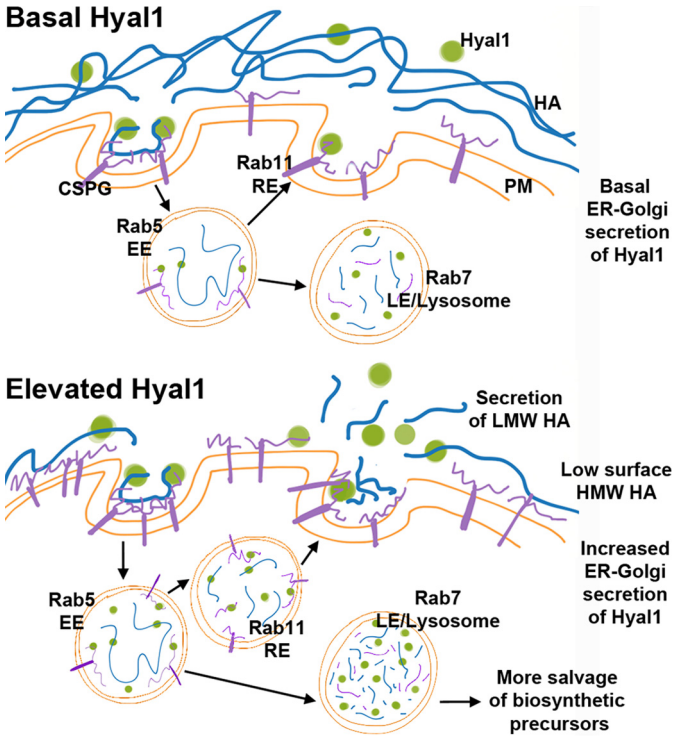

FIGURE 9. **Proposed model for Hyal1 impact on vesicle trafficking and tumor cell motility.** Hyal1 activity is virtually undetectable (basal) in parental 22Rv1 cells, which retain low levels of cell surface high molecular weight (*HMW*) HA and are poorly motile. When Hyal1 activity is elevated by overexpression, the increased secretion of Hyal1 leads to absence of surface high molecular weight HA; increased motility, proliferation, and receptor recycling; and accelerated vesicular trafficking that depends on Hyal1 binding to HA and/or chondroitin sulfate proteoglycans (*CSPG*) and may result in increased nutrient availability for biosynthesis as well as the release of partially digested, biologically potent low molecular weight (*LMW*) HA signals. *EE*, early endosome; *LE*, late endosome; *RE*, recycling endosome; *PM*, plasma membrane.

fragments of HA have been shown to enhance proliferation, motility, and angiogenesis, and an increase in partial HA catalysis to oligomeric fragments resulting from excess vesicular Hyal1-mediated uptake could contribute to the enhanced pro-cancer phenotype we see in the Hyal1-overexpressing cells (9).

Several conserved residues within the Hyal1 protein are important to maintain wild-type activity (19). Specifically, mutation of residue 131 from glutamate to glutamine abolishes all catalytic activity (19), whereas tyrosine to phenylalanine at position 202 maintains maximal catalytic competence only at saturating substrate concentrations. Expression of Hyal1E131Q causes cells to have a reduced proliferation rate and migratory phenotype compared with cells expressing wild-type Hyal1. Utilizing pH-stable fluorescent fusion proteins of the wild type and catalytic mutants, we see that catalytic activity of Hyal1 is actually required for proper localization in the cell, and for the first time, we can visualize its trafficking itinerary through multiple sorted vesicle compartments. It is apparent that Hyal1WT and the Y202F mutant are vesicular in cells at steady state, colocalize with lysosomal tracers and Rab-GFP fusion constructs, and overlap with endosomal EEA1 and lysosomal cathepsin D in sucrose gradient fractions. In contrast, Hyal1E131Q-tdT does not have a significant vesicular localization, correlates with the ER network, and overlaps with the ER marker calnexin in gradient fractions. How the catalytic activity can affect the localization of the Hyal1 protein is not clear, but the partial wild-type behavior of the HA-binding mutant Y202F in 22Rv1 cells suggests some degree of HA or other substrate binding is required for constitutive secretion as well as reuptake (Fig. 9). For example, perhaps the Y202F mutant has an altered ability to bind chondroitin sulfate proteoglycans and is differentially sensitive to competitive binding of excess HA fragments or HA polymers and therefore does not get internalized and trafficked similarly. We detect E131Q protein in the conditioned media so at least a portion is being secreted by the cell, but much of it remains in the ER due to its loss of catalytic function, which likely includes binding.

Imaging the Hyal1 fusion proteins, we also noticed that vesicles containing wild-type Hyal1 seem to be clustered at the focal adhesions of cells. There was no apparent trend seen for the Hyal1E131Q-tdT fusion protein. The creation and diffusion of focal adhesions are instrumental for cell migration, especially in a unidirectional manner. It has been shown that inhibiting HA synthesis in esophageal cancer cell lines causes disruption of focal adhesions (36). Perhaps it is a combination of HA synthesis and degradation and internalization accompanied by the Hyals that actually has the most effect on prostate cancer cells.

Finally, we used different chemicals to perturb common endocytic trafficking mechanisms to see whether localization of Hyal1 was affected in these situations. Brefeldin A, which blocks the transport of proteins from ER to Golgi, does not change the localization of the Hyal1-tdT fusion protein, indicating that it is likely not rapidly turned over. The localization of the Hyal1E131Q-tdT protein was also similar with and without brefeldin A treatment except for a modest intensification of the ER signal, supporting its reduced rate of secretion relative to the wild-type Hyal1. These results are also consistent with ≈10-fold higher expression of Hyal1E131Q-tdT in the cell lysate compared with that of wild-type Hyal1. We used chloroquine to prevent the acidification of late endosomes into lysosomes. Hyal1 is reportedly a lysosomal protein (18) so we are not surprised to see that when we inhibit lysosomal acidification there is a buildup of Hyal1WT-tdT and Hyal1Y202F-tdT in larger sized vesicles compared with control treatment. This again suggests that the Hyal1 is ultimately trafficked into lysosomes and undergoing degradation. However, what is novel is the implication that Hyal1 is trafficked and released back to the plasma membrane without being degraded, so inhibition of this pathway would also cause buildup of protein within the cell by this route. Hyal1E131Q-tdT protein is also affected by chloroquine treatment, which reduces its proteolysis in the cell as well as its overall levels, suggesting that only newly synthesized protein is present prior to secretion. We used bafilomycin A1, an inhibitor of vacuolar ATPases, to prevent fusion of autophagosomes with lysosomes. Treatment of Hyal1WT-tdT cells with bafilomycin A1 induces accumulation of Hyal1 in significantly larger vesicles that are fewer in number. This indicates that the fusion of smaller endocytic vesicles and autophagosomes with lysosomes is prevented and that Hyal1 is intriguingly present in autophagic vesicles, which may be required for engulfment of HA encapsulated cells.

In summary, we have shown that the catalytic activity of Hyal1 is required for its effects on enhancement of cell prolif-

eration and motility. The mechanism involves localization and trafficking of the protein that are dependent on its association with HA and/or chondroitin sulfate ligands during secretion. In addition, the overexpression of wild-type Hyal1 in aggressive prostate tumor cells increases accumulation of internalized HA fragments and overall endocytic rate. This is one mechanism by which accelerated HA turnover influences the presence and activation of cell surface receptors that control cellular metabolic pathways.

References

1. Siegel, R., Ma, J., Zou, Z., and Jemal, A. (2014) Cancer statistics, 2014. *CA Cancer J. Clin.* **64,** 9–29
2. McAtee, C. O., Barycki, J. J., and Simpson, M. A. (2014) Emerging roles for hyaluronidase in cancer metastasis and therapy. *Adv. Cancer Res.* **123,** 1–34
3. Aaltomaa, S., Lipponen, P., Tammi, R., Tammi, M., Viitanen, J., Kankkunen, J. P., and Kosma, V. M. (2002) Strong stromal hyaluronan expression is associated with PSA recurrence in local prostate cancer. *Urol. Int.* **69,** 266–272
4. Anttila, M. A., Tammi, R. H., Tammi, M. I., Syrjänen, K. J., Saarikoski, S. V., and Kosma, V. M. (2000) High levels of stromal hyaluronan predict poor disease outcome in epithelial ovarian cancer. *Cancer Res.* **60,** 150–155
5. Auvinen, P., Tammi, R., Parkkinen, J., Tammi, M., Agren, U., Johansson, R., Hirvikoski, P., Eskelinen, M., and Kosma, V. M. (2000) Hyaluronan in peritumoral stroma and malignant cells associates with breast cancer spreading and predicts survival. *Am. J. Pathol.* **156,** 529–536
6. Franzmann, E. J., Schroeder, G. L., Goodwin, W. J., Weed, D. T., Fisher, P., and Lokeshwar, V. B. (2003) Expression of tumor markers hyaluronic acid and hyaluronidase (HYAL1) in head and neck tumors. *Int. J. Cancer* **106,** 438–445
7. Kramer, M. W., Escudero, D. O., Lokeshwar, S. D., Golshani, R., Ekwenna, O. O., Acosta, K., Merseburger, A. S., Soloway, M., and Lokeshwar, V. B. (2011) Association of hyaluronic acid family members (HAS1, HAS2, and HYAL-1) with bladder cancer diagnosis and prognosis. *Cancer* **117,** 1197–1209
8. Gomez, C. S., Gomez, P., Knapp, J., Jorda, M., Soloway, M. S., and Lokeshwar, V. B. (2009) Hyaluronic acid and HYAL-1 in prostate biopsy specimens: predictors of biochemical recurrence. *J. Urol.* **182,** 1350–1356
9. Bharadwaj, A. G., Kovar, J. L., Loughman, E., Elowsky, C., Oakley, G. G., and Simpson, M. A. (2009) Spontaneous metastasis of prostate cancer is promoted by excess hyaluronan synthesis and processing. *Am. J. Pathol.* **174,** 1027–1036
10. Bharadwaj, A. G., Goodrich, N. P., McAtee, C. O., Haferbier, K., Oakley, G. G., Wahl, J. K., 3rd, and Simpson, M. A. (2011) Hyaluronan suppresses prostate tumor cell proliferation through diminished expression of N-cadherin and aberrant growth factor receptor signaling. *Exp. Cell Res.* **317,** 1214–1225
11. Bharadwaj, A. G., Rector, K., and Simpson, M. A. (2007) Inducible hyaluronan production reveals differential effects on prostate tumor cell growth and tumor angiogenesis. *J. Biol. Chem.* **282,** 20561–20572
12. Eyster, C. A., Higginson, J. D., Huebner, R., Porat-Shliom, N., Weigert, R., Wu, W. W., Shen, R. F., and Donaldson, J. G. (2009) Discovery of new cargo proteins that enter cells through clathrin-independent endocytosis. *Traffic* **10,** 590–599
13. Tammi, R., Rilla, K., Pienimaki, J. P., MacCallum, D. K., Hogg, M., Luukkonen, M., Hascall, V. C., and Tammi, M. (2001) Hyaluronan enters keratinocytes by a novel endocytic route for catabolism. *J. Biol. Chem.* **276,** 35111–35122
14. Harada, H., and Takahashi, M. (2007) CD44-dependent intracellular and extracellular catabolism of hyaluronic acid by hyaluronidase-1 and -2. *J. Biol. Chem.* **282,** 5597–5607
15. Slomiany, M. G., Dai, L., Bomar, P. A., Knackstedt, T. J., Kranc, D. A., Tolliver, L., Maria, B. L., and Toole, B. P. (2009) Abrogating drug resistance in malignant peripheral nerve sheath tumors by disrupting hyaluronan-CD44 interactions with small hyaluronan oligosaccharides. *Cancer Res.* **69,** 4992–4998
16. Slomiany, M. G., Grass, G. D., Robertson, A. D., Yang, X. Y., Maria, B. L., Beeson, C., and Toole, B. P. (2009) Hyaluronan, CD44, and emmprin regulate lactate efflux and membrane localization of monocarboxylate transporters in human breast carcinoma cells. *Cancer Res.* **69,** 1293–1301
17. Kothapalli, D., Zhao, L., Hawthorne, E. A., Cheng, Y., Lee, E., Puré, E., and Assoian, R. K. (2007) Hyaluronan and CD44 antagonize mitogen-dependent cyclin D1 expression in mesenchymal cells. *J. Cell Biol.* **176,** 535–544
18. Puissant, E., Gilis, F., Dogné, S., Flamion, B., Jadot, M., and Boonen, M. (2014) Subcellular trafficking and activity of Hyal-1 and its processed forms in murine macrophages. *Traffic* **15,** 500–515
19. Zhang, L., Bharadwaj, A. G., Casper, A., Barkley, J., Barycki, J. J., and Simpson, M. A. (2009) Hyaluronidase activity of human Hyal1 requires active site acidic and tyrosine residues. *J. Biol. Chem.* **284,** 9433–9442
20. Helms, J. B., and Rothman, J. E. (1992) Inhibition by brefeldin A of a Golgi membrane enzyme that catalyses exchange of guanine nucleotide bound to ARF. *Nature* **360,** 352–354
21. Krogstad, D. J., and Schlesinger, P. H. (1987) The basis of antimalarial action: non-weak base effects of chloroquine on acid vesicle pH. *Am. J. Trop. Med. Hyg.* **36,** 213–220
22. Bowman, E. J., Siebers, A., and Altendorf, K. (1988) Bafilomycins: a class of inhibitors of membrane ATPases from microorganisms, animal cells, and plant cells. *Proc. Natl. Acad. Sci. U.S.A.* **85,** 7972–7976
23. Clague, M. J., Urbé, S., Aniento, F., and Gruenberg, J. (1994) Vacuolar ATPase activity is required for endosomal carrier vesicle formation. *J. Biol. Chem.* **269,** 21–24
24. Hascall, V. C., Wang, A., Tammi, M., Oikari, S., Tammi, R., Passi, A., Vigetti, D., Hanson, R. W., and Hart, G. W. (2014) The dynamic metabolism of hyaluronan regulates the cytosolic concentration of UDP-GlcNAc. *Matrix Biol.* **35,** 14–17
25. Bullen, J. W., Balsbaugh, J. L., Chanda, D., Shabanowitz, J., Hunt, D. F., Neumann, D., and Hart, G. W. (2014) Cross-talk between two essential nutrient-sensitive enzymes: *O*-GlcNAc transferase (OGT) and AMP-activated protein kinase (AMPK). *J. Biol. Chem.* **289,** 10592–10606
26. Vigetti, D., Viola, M., Karousou, E., Deleonibus, S., Karamanou, K., De Luca, G., and Passi, A. (2014) Epigenetics in extracellular matrix remodeling and hyaluronan metabolism. *FEBS J.* **281,** 4980–4992
27. Richardson, D. R. (2005) Molecular mechanisms of iron uptake by cells and the use of iron chelators for the treatment of cancer. *Curr. Med. Chem.* **12,** 2711–2729
28. Koshkaryev, A., Piroyan, A., and Torchilin, V. P. (2012) Increased apoptosis in cancer cells *in vitro* and *in vivo* by ceramides in transferrin-modified liposomes. *Cancer Biol. Ther.* **13,** 50–60
29. Murphy, J. E., Padilla, B. E., Hasdemir, B., Cottrell, G. S., and Bunnett, N. W. (2009) Endosomes: a legitimate platform for the signaling train. *Proc. Natl. Acad. Sci. U.S.A.* **106,** 17615–17622
30. Gilcrease, M. Z. (2007) Integrin signaling in epithelial cells. *Cancer Lett.* **247,** 1–25
31. Ramsay, A. G., Marshall, J. F., and Hart, I. R. (2007) Integrin trafficking and its role in cancer metastasis. *Cancer Metastasis Rev.* **26,** 567–578
32. Caswell, P., and Norman, J. (2008) Endocytic transport of integrins during cell migration and invasion. *Trends Cell Biol.* **18,** 257–263
33. Caswell, P. T., Spence, H. J., Parsons, M., White, D. P., Clark, K., Cheng, K. W., Mills, G. B., Humphries, M. J., Messent, A. J., Anderson, K. I., McCaffrey, M. W., Ozanne, B. W., and Norman, J. C. (2007) Rab25 associates with $\alpha5\beta1$ integrin to promote invasive migration in 3D microenvironments. *Dev. Cell* **13,** 496–510
34. Palamidessi, A., Frittoli, E., Garré, M., Faretta, M., Mione, M., Testa, I., Diaspro, A., Lanzetti, L., Scita, G., and Di Fiore, P. P. (2008) Endocytic trafficking of Rac is required for the spatial restriction of signaling in cell migration. *Cell* **134,** 135–147
35. Sigismund, S., Argenzio, E., Tosoni, D., Cavallaro, E., Polo, S., and Di Fiore, P. P. (2008) Clathrin-mediated internalization is essential for sustained EGFR signaling but dispensable for degradation. *Dev. Cell* **15,** 209–219
36. Twarock, S., Tammi, M. I., Savani, R. C., and Fischer, J. W. (2010) Hyaluronan stabilizes focal adhesions, filopodia, and the proliferative phenotype in esophageal squamous carcinoma cells. *J. Biol. Chem.* **285,** 23276–23284